RESEARCH ARTICLE

[M]acro-molecular
Rapid Communications
www.mrc-journal.de

Check for updates

Donor–Acceptor Adduct-Polydimethylsiloxane-Conjugates for Enhanced Photoswitching in Bulk Polymers

Michèle Clerc, Cem Tekin, Sebastian Ulrich, Rafael V. M. Freire, Stefan Salentinig, Nico Bruns, and Luciano F. Boesel*

Donor–acceptor Stenhouse adducts (DASAs) are a rapidly emerging class of visible light-activated photochromes and DASA-functionalized polymers hold great promise as biocompatible photoresponsive materials. However, the photoswitching performance of DASAs in solid polymer matrices is often low, particularly in materials below their glass transition temperature. To overcome this limitation, DASAs are conjugated to polydimethylsiloxanes which have a glass transition temperature far below room temperature and which can create a mobile molecular environment around the DASAs for achieving more solution-like photoswitching kinetics in bulk polymers. The dispersion of DASAs conjugated to such flexible oligomers into solid polymer matrices allows for more effective and tunable DASA photoswitching in stiff polymers, such as poly(methyl methacrylate), without requiring modifications of the matrix. The photoswitching of conjugates with varying polymer molecular weight, linker type, and architecture is characterized via time-dependent UV–vis spectroscopy in organic solvents and blended into polymethacrylate films. In addition, DASA-functionalized polydimethylsiloxane networks, accessible via the same synthetic route, provide an alternative solution for achieving fast and efficient DASA photoswitching in the bulk owing to their intrinsic softness and flexibility. These findings may contribute to the development of DASA-functionalized materials with better tunable, more effective, and more reversible modulation of their optical properties.

1. Introduction

Polymers containing photochromic dyes have been investigated as materials for various applications ranging from optical data storage to sensors, actuators, biomedical devices, and components in non-linear optics.[1–4] The photoswitching ability and efficiency of photochromes implemented in polymer matrices is thus of great importance in order to further advance their applications and to successfully utilize them as translators of light stimuli to trigger macroscopic property changes in materials. However, achieving efficient and reversible photoswitching in polymer matrices, especially in the bulk, has been an ongoing challenge since kinetics of the photochemical reaction and other properties of the photochromes are often strongly influenced by properties of the matrix environment, importantly rigidity, free volume and polarity.[3–7]

Donor–acceptor Stenhouse adducts (DASAs) are a new class of photochromes, which have received increasing attention since their discovery in 2014.[8–10] DASAs undergo a visible light-induced, colored to colorless, open triene to closed cyclopentenone isomerization that is thermally reversible.[11–15] Their tunable absorption in the spectral range between 450 and 750 nm[16–21] enables DASA activation at wavelengths suitable for biological applications.[22] DASA-functionalized polymers were already investigated for potential applications in a number of areas ranging from photo-/hydrochromic,[23–25] photopatternable,[26–29] or wettability switching[30–34] surfaces and objects, to smart drug delivery,[35–40] chemical sensing,[41–45] and photoactuation.[46] Systems operating in suspension, including polymer-based micelles,[35,38,39,47] polymersomes[37] and other polymer nanoparticles,[36,40,43] as well as DASA immobilization in polymer films,[23,31,46] polymer

M. Clerc, C. Tekin, S. Ulrich, L. F. Boesel
Empa, Swiss Federal Laboratories for Materials Science and Technology
Laboratory for Biomimetic Membranes and Textiles
Lerchenfeldstrasse 5, St. Gallen 9014, Switzerland
E-mail: luciano.boesel@empa.ch
M. Clerc, R. V. M. Freire, S. Salentinig
Department of Chemistry
University of Fribourg
Chemin du Musée 9, Fribourg 1700, Switzerland
M. Clerc, N. Bruns
Department of Pure and Applied Chemistry
University of Strathclyde
Thomas Graham Building, 295 Cathedral Street, Glasgow G1 1XL, UK

**ADVANCED
SCIENCE NEWS**

www.advancedsciencenews.com

**Macro-
molecular
Rapid Communications**

www.mrc-journal.de

networks,[24] polymer nanofibers[45] and on functionalized polymeric surfaces[26,30,33,48] were reported.

Structural synthetic modifications for designing DASAs with predictable responses and improved photoswitching properties have led to the development of different DASA generations.[9,16,18] However, their characteristics in solution are rarely consistently replicable in a polymer matrix, especially in the solid state.[23,47,49] DASA photoswitching behavior is profoundly influenced by the molecular environment surrounding the DASAs.[16–18,23,50,51] Medium polarity, for example, heavily influences the spectral and kinetic properties and the thermodynamic equilibrium of DASAs, also in solid polymers.[51] Besides polarity, earlier work in our groups showed that the photoswitching kinetics of DASAs conjugated to the side chains of different poly(meth)acrylates clearly correlated with the rigidity of the polymer in the solid state (fast switching and recovery in polymers above their glass transition temperature, T_g, versus slow and incomplete switching and recovery in polymers below T_g).[23] Similarly, in our DASA-functionalized networks based on thiol-ene photo resins, softer, less cross-linked networks showed faster photoswitching responses.[24] This is not surprising since the photoisomerization from the extended open triene isomer to the more compact cyclopentenone isomer involves significant changes in molecular shape and volume. A glassy polymer may prohibit the molecular mobility that is required for this process. This becomes particularly relevant in the design of materials that have to impart stringent mechanical requirements and still preserve photoswitching capacity. Stenzel and co-workers recently investigated the effect of polymer chain length and polymer backbone in a series of polyacrylate and polymethacrylate DASA-functionalized homopolymers in solution.[47] Both chain length and backbone of the polymer led to differences in the switching ability of DASAs supporting previous findings that even small changes in the local environment caused by the polymer can result in significant changes in the DASA photoswitching properties. In addition to the intrinsic characteristics of the polymer, the mode of incorporation (dissolution or covalent attachment, linker type, macromolecular architecture) can also affect a photochrome's behavior.[5–7]

The increasing interdisciplinary interest in DASA-based materials requires a more detailed understanding of DASA behavior in macromolecular systems, as well as to overcome photoswitching limitations of DASAs in the solid state[23,49] and in aqueous environment.[52] Besides structural modifications of the DASA itself, "add-on" methods such as nanoencapsulation and conjugation to cleverly engineered polymers are complementary approaches that can improve and sustain DASA photoswitching performance in functional materials. The photoswitching kinetics and dark equilibrium of DASAs can be modulated without altering their intrinsic structure and electronic properties through directed changes of the DASA local environment. This idea of "externally" tuning DASA photoswitching properties through, for example, electrostatic and specific interactions (H-bonding), was demonstrated in different literature studies, ranging from small molecule additives[21] to intricate Hamilton-type hydrogen bonding receptors.[53] A shielding of the DASAs from the bulk medium was also demonstrated in the form of metal-ligand based molecular vessels,[54] supramolecular complexes with organic host macrocycles,[55,56] and nanocages of metal-organic frameworks (MOFs).[57] In this context, Evans

and co-workers[58,59] achieved tunable photoswitching kinetics inside rigid polymers for spirooxazines,[59–61] azo dyes,[59] and chromenes[59,61–65] by covalently attaching short polymer chains with desirable properties to these photochromes before embedding them inside matrix polymers.[58,59] It was postulated that the attached short-chain polymer can create an immediate environment of controlled rigidity and polarity around the photochromes as a form of nanoencapsulation.[58,59] This protects the photochromes from the bulk matrix and thereby alters their photoswitching capacity without significantly affecting their electronic properties or the physical/mechanical properties of the bulk.[58,59]
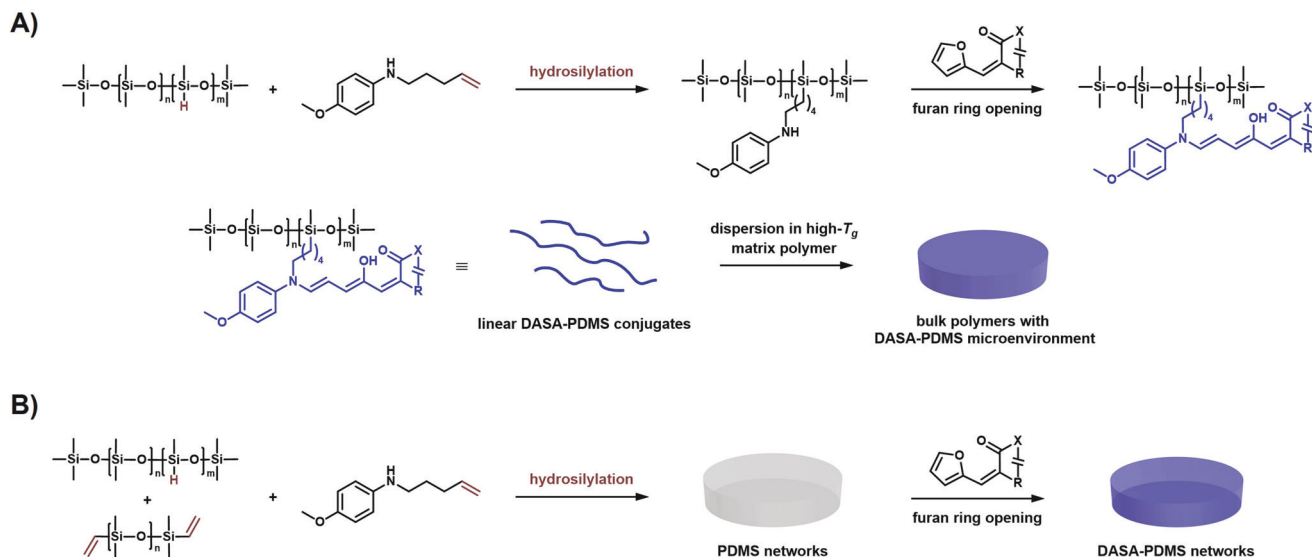
Inspired by Evan's studies,[58,59] we envisioned that the attachment of DASAs to polymers with a low T_g could be used as a general method to systematically tune DASA photoswitching inside a rigid host polymer without requiring bulk modification of the matrix. Thus, DASAs were covalently conjugated to polydimethylsiloxane (PDMS) due to the high mobility and flexibility of this polymer (T_g, of −150 to −120 °C)[66] possibly allowing for a low-T_g microenvironment[61] to "cushion" the DASAs inside the rigid bulk polymers. A series of DASA-PDMS conjugates was synthesized via platinum-catalyzed hydrosilylation of alkene-functional DASA-precursors with commercially available linear poly(dimethyl-methylhydro)siloxanes. The photoswitching of these conjugates was characterized in solution and in solid polymethacrylate films using time-dependent UV–vis spectroscopy. The polymer films are further analyzed with profilometry, confocal Raman microscopy and atomic force microscopy to characterize their micro- and nanostructure. Additionally, the hydrosilylation conjugation approach enables access to not only DASA-functionalized linear polymers, but also DASA-functionalized PDMS networks. These networks allow for fast and efficient DASA photoswitching due their hydrophobicity, optical clarity and intrinsic softness and are presented as an alternative solution for overcoming the limitations in utilizing DASAs inside bulk materials.

2. Results and Discussion

2.1. Synthesis of Linear DASA-PDMS Conjugates

DASA-PDMS conjugates were synthesized in a two- or three-step procedure from linear poly(dimethyl-methylhydro)siloxanes (**Scheme 1**), a class of compounds manufactured on a large scale for the silicone industry. These compounds are commercially available in a range of different molecular weights and hydrosilane contents. In this way, DASA-functional polymers with predefined architectures and molecular weights can be easily and rapidly accessed by hydrosilylation, the "native" conjugation chemistry of silanes and polysiloxanes. A broad scope of alkene- or alkyne-bearing compounds can be applied in the hydrosilylation reaction to efficiently functionalize a variety of silicon based materials, from polysiloxane oils and networks to organofunctional alkoxysilanes for the silanization of glass surfaces.[67,68]

As detailed in **Scheme 2**, two different alkene-functional aromatic secondary amine precursors (1 and 2) and an alkene-functional barbituric acid acceptor (3) were used for the addition to a library of different poly(dimethyl-methylhydro)siloxanes under Karstedt's platinum catalysis in toluene at 60 °C overnight

ADVANCED
SCIENCE NEWS
www.advancedsciencenews.com

[M] acro-
molecular
Rapid Communications
www.mrc-journal.de

A)

B)

Scheme 1. General overview on covalent conjugation of DASAs to (poly)siloxanes/silanes by hydrosilylation of alkene-functional DASA-precursors with hydrosilane groups and subsequent reaction with furan adducts. A) The synthesis is applicable to poly(dimethyl-methylhydro)siloxanes for the preparation of linear DASA-PDMS conjugates, which can then be blended into rigid host polymers. B) DASA-functionalized PDMS networks can be prepared through simultaneous crosslinking and alkene-precursor integration during the hydrosilylation step and subsequent reaction with the furan adducts.

	Length	Acceptor
M1-barb	$n \sim 15$	4
M1-pyra	$n \sim 15$	5
M2-barb	$n \sim 110$	4
M2-pyra	$n \sim 110$	5
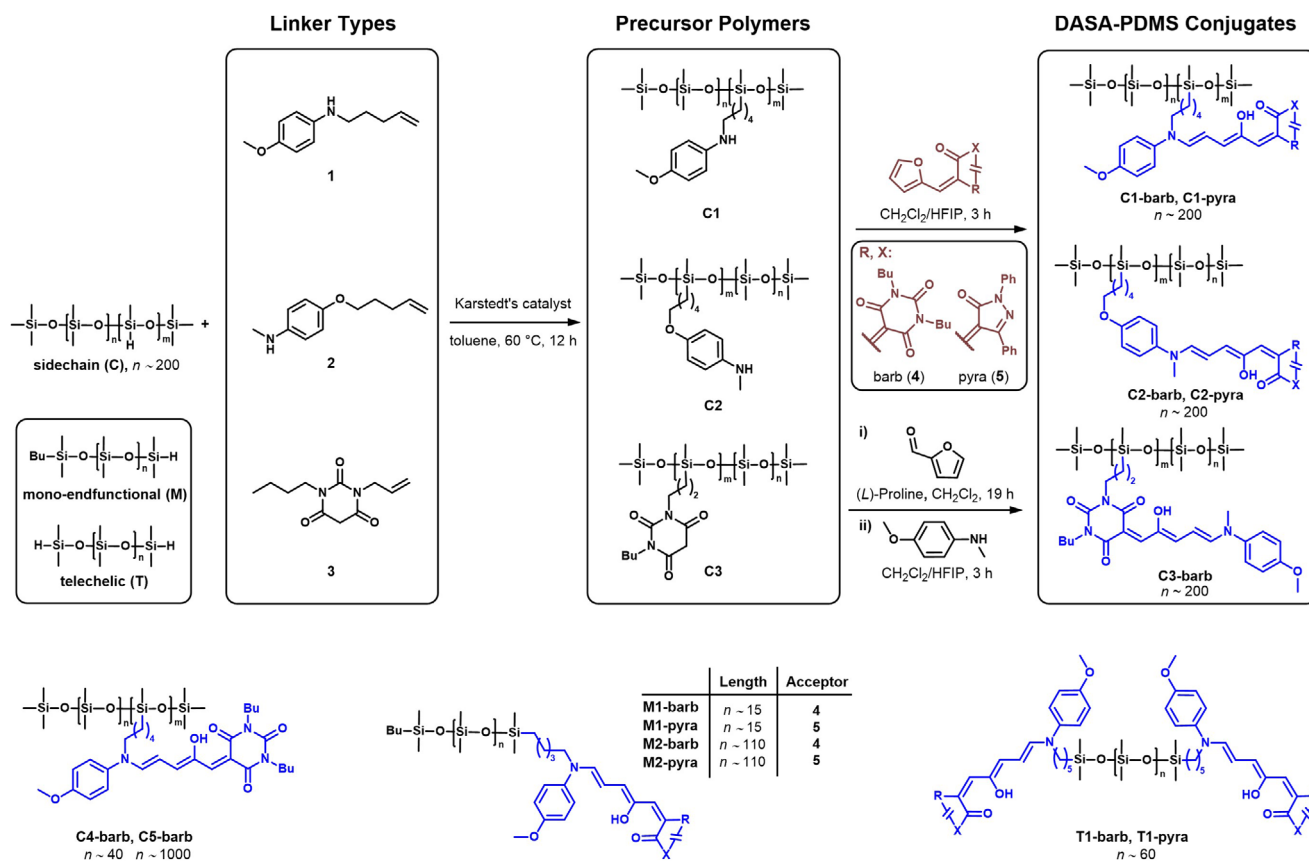
Scheme 2. Synthetic route to DASA-PDMS conjugates used in this study. The synthesis comprises of a two- or three-step approach via precursor integration by platinum-catalyzed hydrosilylation chemistry on commercially available hydrido-functional polydimethylsiloxanes. Note: The side-chain functional polymers are random copolymers of dimethylsiloxane and methylhydrosiloxane. For simplicity, only the open form of the DASA is shown. However, the DASAs exist as a mixture of open and closed cyclopentenone isomers at thermodynamic equilibrium.

ADVANCED
SCIENCE NEWS
www.advancedsciencenews.com

[M] acro-molecular
Rapid Communications
www.mrc-journal.de

Table 1. Library of polymers investigated in this study.

Formula number[a]	Linker type	Average nr. of functional groups per chain[b]	M_n [g mol^{-1}], Đ (GPC)[c] Precursor polymer
Side-chain functional (C):			
C1-barb	1	6.1	15 600, 2.0
C1-pyra			
C2-barb	2	6.1	16 700, 1.7
C2-pyra			
C3-barb	3	6.1	11 500, 2.1
C4-barb	1	0.9	3200, 1.5
C5-barb	1	5.5	88 700, 1.7
Mono-endfunctional (M):			
M1-barb	1	1.0	800[d]
M1-pyra			
M2-barb	1	1.0	8700, 1.3
M2-pyra			
Telechelic (T):			
T1-barb	1	2.0	4500, 1.3
T1-pyra			

[a] The nomenclature involves a letter designating the functional group attachment on the polymer followed by a sequential numbering of the different polymers. "-barb" labels compounds containing DASAs based on barbituric acid 4, while "-pyra" labels DASAs derived from pyrazolone 5; [b] Calculated for the unfunctionalized polymers from the information given by the manufacturer; [c] Dispersity (Đ) and number average molecular weight (M_n) were measured by gel permeation chromatography (GPC) in THF with narrow PDMS standards. The results on the precursor polymers obtained after hydrosilylation are reported since DASA functionalities can lead to measurement artefacts[47] probably due to sample-to-column interactions; [d] M_n determined by ^{1}H NMR spectroscopy.

(synthetic procedures and characterization in Experimental Section and Sections S1,S2, Supporting Information). Different number average molecular weights (M_n ≈1000–90 000 g mol^{-1}) and architectural configurations (sidechain, mono-endfunctional, and telechelic) were investigated. The precursor polymers obtained after hydrosilylation will be designated hereafter as C1-C5 (sidechain functional), M1 and M2 (mono-endfunctional), and T1 (telechelic), with details given in **Table 1**.

In a second step, the amine-modified precursor polymers were subjected to reaction with an excess of furan adducts (4 or 5) affording strongly colored DASA-PDMS conjugates as waxy solids or viscous oils. This two-step approach also has the advantage of providing access to different DASA derivatives in the same material by varying the reagent in the second step. We demonstrate this by synthesizing barbituric acid based (4, denoted with "-barb") second generation DASAs, as well as a third generation pyrazolone-derived (5, "-pyra") DASAs from the same amine precursor polymers.

Compound C3-barb comprises DASAs that are conjugated to the PDMS chain via the acceptor unit and was synthesized in three steps (Scheme 2). This procedure, although resulting in DASA-functionalized polymers, is inferior to the aforementioned method via amine-precursor polymers, as it resulted in lower degrees of DASA-functionalization presumably caused by DASA degradation during the reaction with the excess amine compo-

nent in the last step. Moreover, direct conjugation via hydrosilylation of an alkene-functional furan adduct or an alkene-functional DASA employing Karstedt's catalyst was attempted, but a significant degree of side reactions on the non-terminal double bonds of the furan adduct or the DASA triene renders this strategy impractical (Section S2.4.4, Supporting Information).

The DASA formation on the precursor polymers could be strongly promoted by performing the reactions in dichloromethane (CH_2Cl_2) containing 1,1,1,3,3,3-hexafluoro-2-propanol (HFIP, 20 vol%) as a co-solvent at room temperature. These reaction conditions, previously developed in our group, substantially increase the practicality of multi-step DASA synthesis on polymers by accelerating the nucleophilic furan ring opening, which substantially reduces the required reaction time.[21] PDMS is stable under these conditions, although prolonged incubation should be avoided as PDMS can be susceptible to acid degradation (Figures S1,S2, Supporting Information).[66] The precursor polymers and DASA-PDMS conjugates were purified from small-molecule impurities by size exclusion chromatography and characterized by nuclear magnetic resonance spectroscopy (NMR), attenuated total reflectance Fourier transform infrared (ATR-FTIR) spectroscopy and gel permeation chromatography (GPC) (**Figure 1**; Supporting Information, Section S2 and Figures S3–S60, Supporting Information).

2.2. DASA-PDMS Conjugates in Solution

To assess the photoswitching behavior of the DASA-PDMS conjugates, dilute solutions with a target DASA concentration of ≈10 μM (Tables S3,S4, Supporting Information) were prepared in THF and equilibrated for at least three hours in the dark before measurements. To evaluate the effect of the polymer conjugation, comparison with a small molecule control DASAs resembling closely the DASA conjugated to the polymers is necessary. DASA model compounds Barb-1, Barb-2, and Pyra were selected for this purpose (Figure 1B). The DASA-PDMS conjugates are intensely purple or blue colored with UV–vis absorbance spectra in solution matching those of the analogous unconjugated DASAs with λ_{max} at 583 nm, 587 nm, and 609 nm, respectively (Figure 1D). For the photoswitching experiments, in situ visible light irradiation within the absorption band of the open isomer (light emitting diodes, LEDs, with nominal wavelengths of 505 nm and 530 nm, Table S2, Figures S61–S63, Supporting Information) leads to isomerization to the colorless cyclopentenone isomer, which can be followed by monitoring the exponential absorbance decay near λ_{max} with UV–vis spectroscopy overtime until the photothermal stationary state (PTSS)[69] is reached (**Figure 2**). Subsequent removal of the light stimulus leads to a thermal equilibration and recovery to the open isomer accompanied by a time-dependent increase in the absorption. The apparent half-lives of the closed isomer ($t_{1/2}$) varies from seconds to hours for different DASA derivatives.[18]

The photoswitching of conjugates based on the same polymer but different linker types (1, 2, or 3, Scheme 2) was analyzed. Even though the electronic ground state properties of the respective barbituric acid based DASAs are expected to be similar, a distinct impact on the kinetics of both the forward reaction and thermal recovery was found, indicating that steric factors may play an
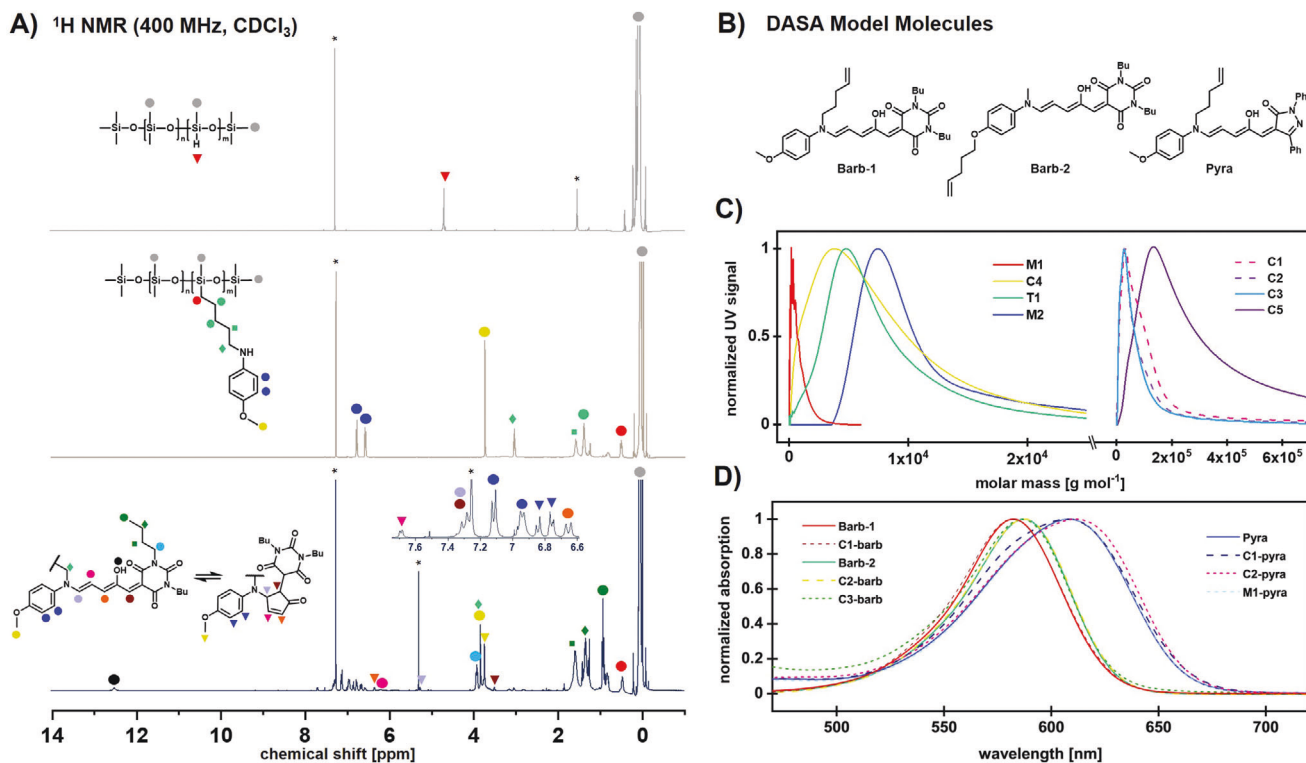
ADVANCED
SCIENCE NEWS
www.advancedsciencenews.com

Macro-
molecular
Rapid Communications
www.mrc-journal.de

Figure 1. Selected characterization data for DASA-PDMS conjugates and precursor polymers and chemical structures of model DASA molecules used as references in this study. A) ^{1}H NMR (400 MHz, 298 K, CDCl$_3$) spectra of C4-barb and its precursors. The DASAs exist as a mixture of open and closed isomers at thermal equilibrium. Residual solvent signals are marked with an asterisk. B) Structures of DASA model molecules. C) Mass distributions of the precursor polymers determined by GPC in THF relative to narrow polydimethylsiloxane standards. D) Normalized UV–vis spectra in THF of DASA-PDMS conjugates and of the model DASAs. For compounds synthesized from linker 1 a λ_{max} at 583 nm for the barbituric acid derivatives can be observed and a λ_{max} at 609 nm for the pyrazolone derivatives. Relative to this, compounds derived from linkers 2 or 3 have 3–4 nm red-shifted absorption maxima.

additional role (Figure 2B; Table S3, Supporting Information). For C1-barb the isomerization under illumination was slower than for C2-barb and C3-barb, while its thermal recovery was markedly faster with an ≈30% decrease in $t_{1/2}$ of the closed isomer. The same trends were also observed for the model DASAs (Barb-1 and Barb-2, Figure S64, Supporting Information) suggesting that the spacer group itself is largely responsible for the observed effect. Studies by Beves and co-workers demonstrated before that sterically bulky substituents on the donor amine (as in linker 1) affect the photoswitching kinetics and thermodynamic dark equilibrium, especially disfavoring the ring closing step.[19] Related to this, for a second generation Meldrum's acid derived DASA based on linker 1 (Figure S14, Supporting Information) we additionally observed the presence of another conformer of the open isomer at room temperature by ^{1}H NMR spectroscopy. This is likely from restricted rotation around the bond between nitrogen center and triene system,[17,19] which was not observed before in a non-bulky *N*-methyl substituted version.[17] Steric hindrance may limit a faster interconversion between these two conformers further underlining the importance of steric factors in addition to electronic factors and the necessity to consider these in the linker design for DASA integration into macromolecular systems.

Among the majority of barbituric acid DASA-conjugates with the same linker type (Figure 2C,D) little variations in the forward isomerization and recovery kinetics in THF were found,

irrespective of the differences in molecular weights and architectures. The half-lives of the closed isomer for all these conjugates are within less than ±5% of the small molecule model Barb-1 (Table S3, Supporting Information). An exception was the highest molecular weight conjugate C5-barb that also has the lowest functionalization percentage, which recovered markedly faster. On the other hand, for the pyrazolone derivatives (Figure 2E) all PDMS conjugates recovered faster than model DASA Pyra and the recovery speed increases with increasing molecular weight (except for the telechelic conjugate T1-pyra that falls out of line as it recovered the fastest). These results indicate that PDMS conjugation has no notable deaccelerating effect on DASA thermal recovery in THF solution. It is likely that for PDMS, a very flexible and soft polymer that is well soluble in THF, steric restrictions on the DASA isomerization imposed by polymer conjugation are negligible and factors other than backbone rigidity and molecular mobility restrictions governing behavior in many bulk polymers[23,24] are more decisive in the solvated state, in line with previous observations.[47] These other factors may include local medium polarity changes, as well as inter-/intramolecular interactions of DASAs with the polymer and other DASAs. Interestingly, it was recently reported that the polarity sensitivity and concentration dependence of the photoswitching kinetics vary for different DASA generations, probably as a result of the different ionic characters of their open and closed isomers.[51] Second
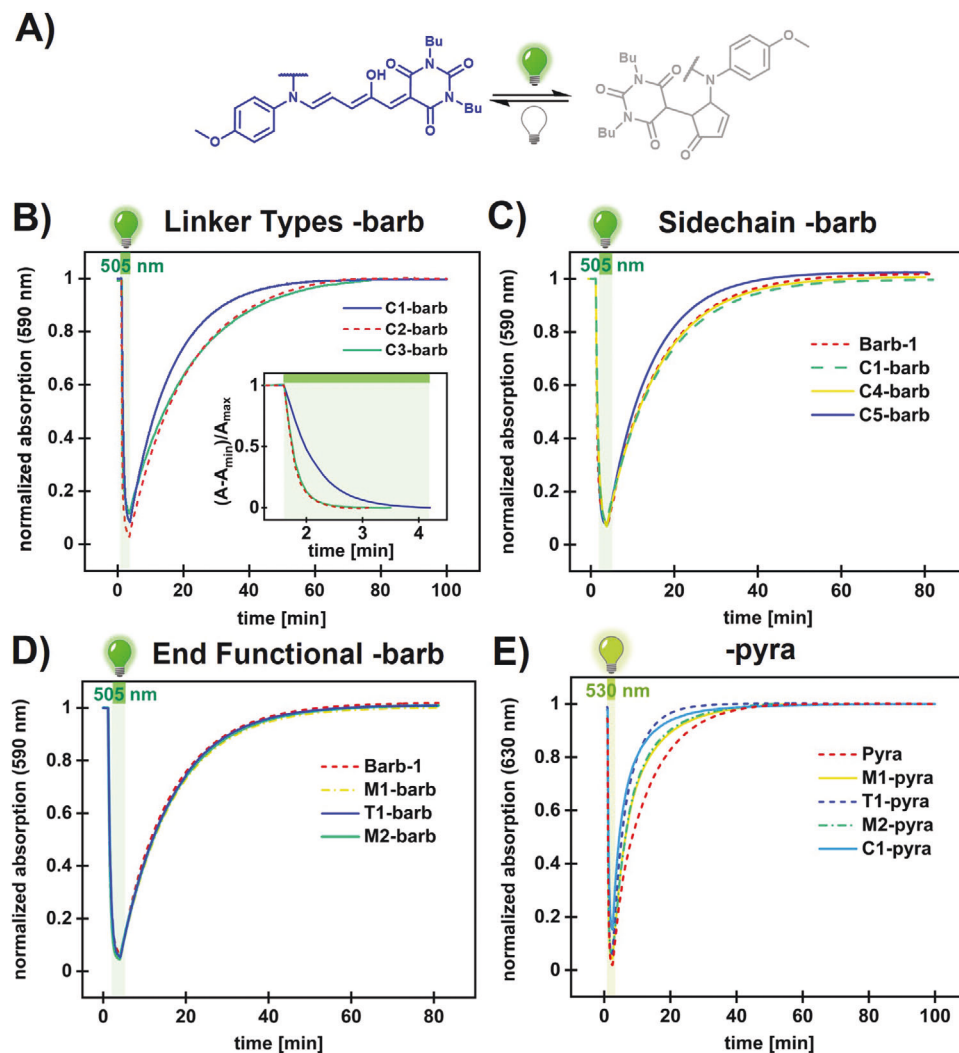
ADVANCED
SCIENCE NEWS
www.advancedsciencenews.com

[M] macro-
molecular
Rapid Communications
www.mrc-journal.de

Figure 2. Photoswitching experiments of DASA-PDMS conjugates in THF solution compared to the corresponding model DASAs. A) Chemical structures of open and closed isomers of barbituric acid DASA based on linker 1. The closed isomer is depicted with the acceptor in the keto form, but it can also reside in an enol or zwitterionic state.[51] B) Time-dependent UV–vis spectroscopy at 590 nm for conjugates derived from different linkers (1, 2, or 3) during forward switching under illumination (505 nm) and during thermal recovery in the dark. Inset shows the forward switching kinetics. Time-dependent UV–vis spectroscopy at 590 nm for the barbituric acid derived C) sidechain- and D) end- functional conjugates during forward switching under illumination (505 nm) and during thermal recovery in the dark. E) Time-dependent UV–vis spectroscopy at 630 nm for the pyrazolone derivatives during forward switching under illumination (530 nm) and during thermal recovery in the dark.

generation DASAs (such as Barb-1 and Barb-2) are less sensitive to medium polarity changes in contrast to most third generation DASAs,[51] which could explain why the third-generation pyrazolone-based conjugates applied herein (C1-pyra, M1-pyra, M2-pyra, and T1-pyra) deviate more strongly in their behavior from the model DASA even for short-chain polymer attachment.

In addition, the influence of the type of linker and of PDMS conjugation on the thermodynamic equilibrium of the DASAs in the dark was determined by ^{1}H NMR in CDCl$_3$ at room temperature. For Barb-1 and the respective PDMS-conjugates it was observed that the open isomer is strongly stabilized over the closed isomer when compared to Barb-2 and its conjugates ($\approx$65% open versus $\approx$35% open, Figures S65,S66, Supporting Information). This is likely related to the sterically demanding substituents on the donor nitrogen present in the former group, which disfa-

vors conversion to the closed isomer, in accordance with previous findings.[19,21] The polymer conjugation, however, was found to have no or only a minor effects on the dark equilibrium in CDCl$_3$.

2.3. DASA-PDMS Conjugates in Matrix Polymers

DASA-PDMS conjugates could allow for enhanced DASA photoswitching in solid polymers that would otherwise impede photoswitching. Thus, the photochromic behavior of selected DASA-PDMS conjugates was investigated in solid polymer films (**Figure 3**A). Commercially available polymethyl methaclyte (PMMA), poly(ethyl methacrylate) (PEMA), and poly(butyl methacrylate) (PBMA) (T_g of 90 °C, 71 °C, and 31 °C,
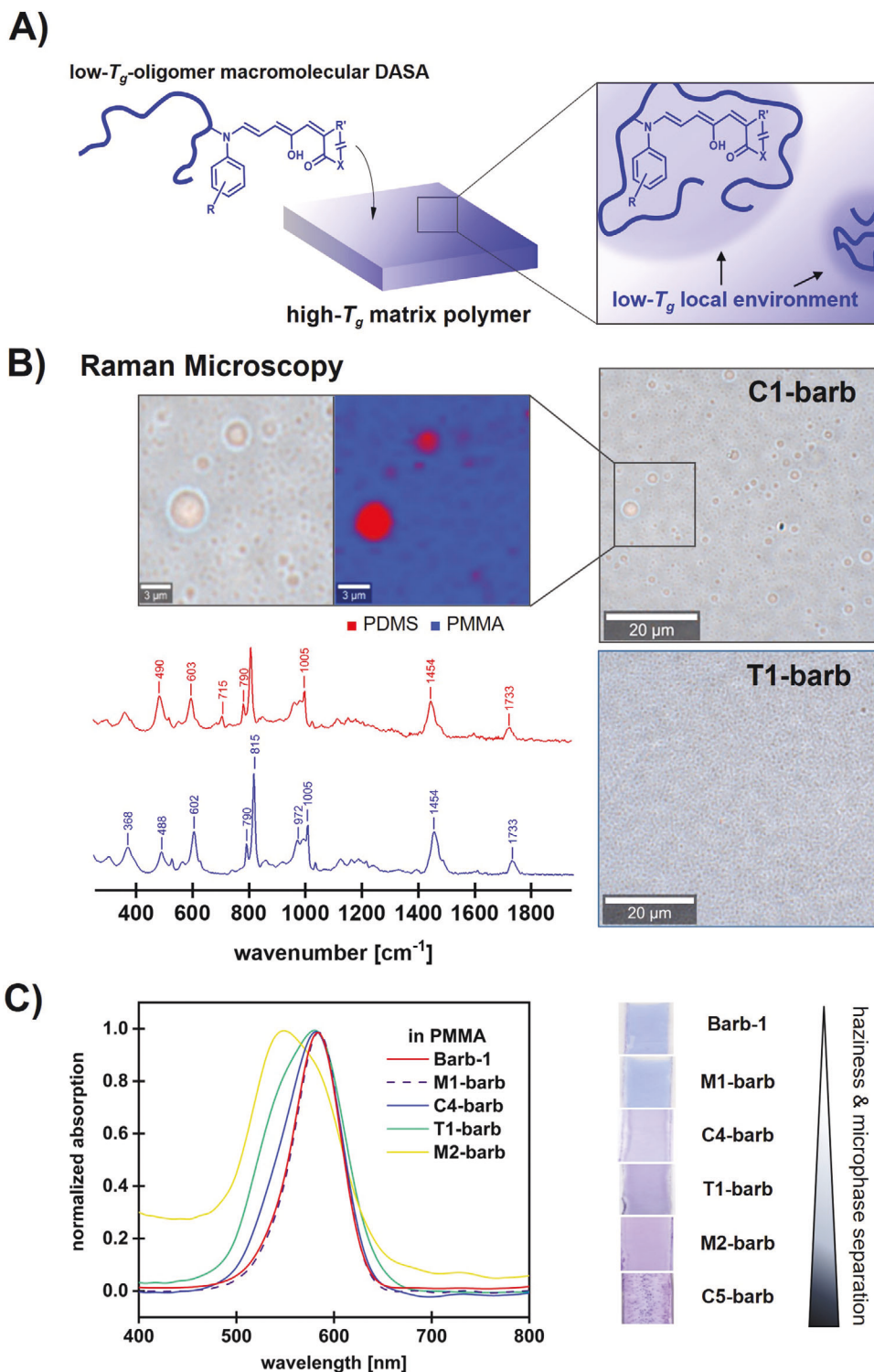
Figure 3. DASA-PDMS conjugates in PMMA films. A) Schematic depiction of the concept to create a PDMS microenvironment around the DASAs within a PMMA matrix. B) Confocal Raman microscopy image for a PMMA film containing conjugate C1-barb displaying microphase separation observed for higher molecular weight conjugates. In the red regions of the compositional images, the bands at 490 cm^{-1} and 715 cm^{-1} indicative for PDMS are more intense. Microscopy image of T1-barb for comparison, which does not show microphase separation. C) UV–vis spectroscopy (transmission mode) and photographic images of the PMMA films. Higher molecular weight conjugates led to increased phase separation with the matrix polymers.

**ADVANCED
SCIENCE NEWS**

www.advancedsciencenews.com

Macromolecular
Rapid Communications

www.mrc-journal.de

respectively, determined by differential scanning calorimetry, DSC, Table S5, Supporting Information), were chosen as matrix polymers since highly transparent solid films can be easily prepared from these materials and the polymers are aprotic in nature (in protic media DASA cyclization independently of light is observed[10]). For the production of optically clear films, the matrix polymer and the DASA-PDMS conjugate were dissolved in toluene or toluene/CH_2Cl_2 mixtures and dip-coated onto glass slides delivering polymer films with thicknesses between 6.5 and 7 μm from profilometry (Figure S67, Supporting Information). Different contents of DASA-PDMS conjugate (0.5–7 wt%) were used depending on their molecular weights in order to achieve comparable DASA concentrations in the films (Table S6, Supporting Information). For comparison, polymer films that contained the free DASAs were prepared in the same way.

High molecular weight PDMS-conjugates (M_n > 10 000 g mol^{-1}) lead to a hazy appearance of the polymer films most likely from the formation PDMS domains inside the matrix polymer that are large enough to scatter light (Figure 3). For the samples with M_n < 10 000 g mol^{-1}, however, optically homogenous films could be obtained. DSC measurements on films prepared with the conjugates of the latter group, for example T1-barb, showed no significant changes in the T_g of the matrix polymer demonstrating that no softening of the matrix occurred (Table S5, Supporting Information).

The polymer films were further analyzed with confocal Raman microscopy, atomic force microscopy (AFM), and UV–vis spectroscopy to evaluate their micro- and nanostructure and the optical properties. Due to the covalent attachment of the DASAs to the PDMS, it is suggested that within the matrix polymers the PDMS chain entangles and coils to varying degrees around the DASAs resulting in films where the photoswitches are located within the PDMS phase or at the interface between the PDMS and the matrix polymer.[58,59] This modifies the local environment in direct proximity around the DASAs. Alternatively, it is also possible that distinct phases of multiple DASA-PDMS conjugates form within the matrix polymer owing to phase separation of the two types of polymer, especially at higher concentrations. For the optically transparent samples, these segregated structures, with their distinct refractive indexes, need to be confined to the nanoscale (<200 nm). For larger domains in the dimension of the wavelength of visible light, turbidity (haze) will appear owing to multiple-scattering of the light amongst them. In agreement with the qualitative observations made before, confocal Raman microscopy revealed μm-sized PDMS domains for films with high-M_n-conjugates M2-barb and C1-barb, whereas in films containing M1-barb and T1-barb no such aggregates on a micrometer level were detectable (Figure 3B; Figures S68–S72, Supporting Information).

For example, PMMA films containing conjugate C1-barb show domains > 1 μm, for which the bands in the Raman spectrum at 490 cm^{-1} and 715 cm^{-1}, indicative for PDMS (Si–O and C–Si–C symmetric stretches, respectively),[70] are significantly more intense as in the surrounding regions (Figure 3B). AFM analysis of the film surface revealed higher surface roughness with increasing molecular weight of the conjugates, again indicating higher degrees of microphase separation (Figure S73 and Table S7, Supporting Information), however, distinct PDMS domains in the sub-micrometer range for the films containing low molec-

ular weight conjugates could not be detected. Increasing the average molecular weights of the PDMS-conjugates also led to visible differences in the color of the films with a gradual change from bluish toward more purple (Figure 3C), which suggests differences in the polarity of the immediate DASA environment[51] or possibly aggregation.[49] DASAs are strongly solvatochromic with their absorption being blue-shifted in, for example, solvents and solid macromolecular environments of higher polarity.[51] Interestingly, DASAs covalently attached to PDMS networks (vide infra) also appear more purple to the naked eye in the dry state as compared to the same network swollen in chloroform or THF. UV–vis spectroscopy on the PMMA films (transmission mode, Figure 3C) showed that Barb-1, M1-barb, C4-barb (M_n < 3500 g mol^{-1}) in PMMA have UV–vis absorbance spectra similar to DASA-PDMS conjugates in solution, while T1-barb and M2-barb show band broadening and an enhancement of the vibronic features[20,49,71] at shorter wavelengths, especially for conjugate M2-barb. Increased background absorbance for M2-barb over large parts of the spectrum also reflect the compromised film transparency.

The efficacy of this approach therefore clearly depends on the compatibility of the polymer attached to the DASA and of the DASA itself with the matrix polymer. For PDMS, a polymer with very low compatibility with polymethacrylates, the average molecular weight of PDMS-based macromolecular DASAs appears to be limited to rather short chains of M_n < 3000 g mol^{-1} in order to avoid excessive phase separation in the applied concentration range.

2.4. Photoswitching of DASA-PDMS Conjugates in Matrix Polymers

Due to steric constraints from the limited free volume available and the reduced segmental motion of macromolecules, photoswitching in general is slower and more complex in bulk polymers as compared to in solution.[5,7] To evaluate the application of DASA-PDMS conjugates in improving the photoswitching performance of DASAs in rigid polymers, the photoswitching kinetics of selected conjugates in polymethacrylate films were compared to analogous films containing the unconjugated model DASA. In accordance with previous findings,[23,49] the forward switching of Barb-1 in PMMA at room temperature is strongly impeded by the matrix and the time spans required to reach half of the initial absorption value ($t_{A1/2}^P$) under irradiation is >30 min (**Figure 4**). The recovery kinetics in the dark (Figure 4A) is even more compromised when compared to solution measurements, whereby the limited recovery to the original open/closed equilibrium might indicate a trapping of the closed isomer inside the glassy matrix and potentially some degree of photodecomposition due to the longer irradiation times required to reach the PTSS. Interestingly, for both the forward switching and the thermal recovery in PMMA films an initial fast component was observed. This deviation from first-order behavior, which is normally observed for DASAs in dilute solutions, has been reported before for azobenzene and spiropyran containing polymers and was explained in terms of the non-uniform distribution of free volume in glassy polymers or non-uniform interactions with the polymer polar groups.[5–7] To account for this, the photoswitching
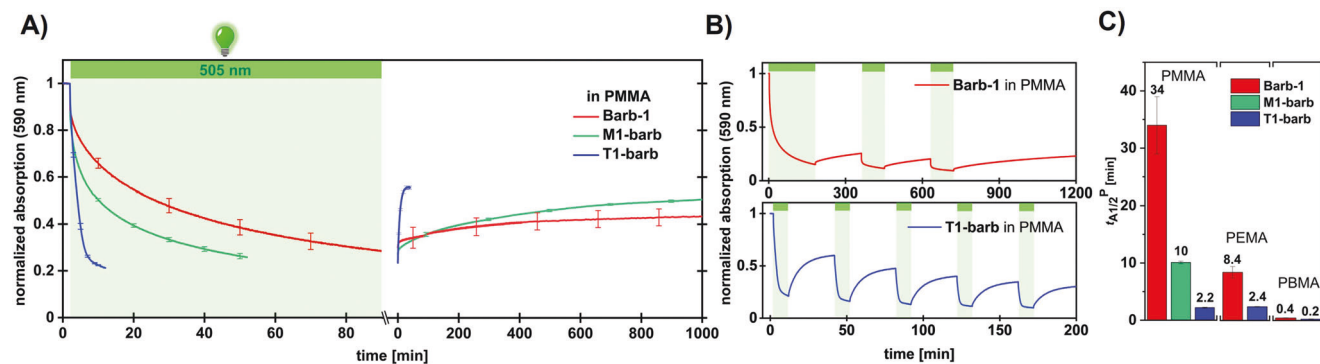
**ADVANCED
SCIENCE NEWS**

www.advancedsciencenews.com

⎰M⎱ **acro-
molecular**
Rapid Communications

www.mrc-journal.de

Figure 4. Photoswitching experiments of DASA-PDMS conjugates and reference model DASA in polymethacrylate films at room temperature. A) Time-dependent UV–vis spectroscopy at 590 nm during forward switching under illumination (505 nm) and thermal recovery in the dark in PMMA films. The measurements were performed in triplicates with the standard deviation displayed at selected time points in the graph. The samples were irradiated until the absorbance decay markedly slowed down. B) Time-dependent UV–vis spectroscopy (590 nm) with repeating cycles of illumination (505 nm) and thermal recovery in the dark in PMMA. C) Time spans required to reach half of the initial absorption values ($t_{A1/2}{}^{P}$) under illumination (505 nm) in PMMA, PEMA, and PBMA.

data in films was fitted with an empirical biexponential model (coefficient of determination $R^2 > 0.99$, Section S10, Supporting Information).

Conjugates M1-barb and T1-barb clearly presented a superior photoswitching performance in PMMA than model DASA Barb-1 (Figure 4). The macromolecular DASA photoswitches switched faster under light irradiation and the thermal recovery percentage is increased from approximately 40% up to 60% for T1-barb. Interestingly, in contrast to the multi-exponential behavior observed for Barb-1 in polymers at temperatures below T_g, the kinetics for the higher molecular weight PDMS-conjugates in PMMA approach a single exponential behavior as observed in solution and soft polymers. Cycling experiments with conjugate T1-barb or Barb-1 in PMMA demonstrate that the photoswitching capacity for the macromolecular DASA is markedly better, allowing for several cycles to be performed in the time span Barb-1 required irradiation in the first cycle (Figure 4B). A longer PDMS chain is expected to promote higher "encapsulation" efficiency and therefore more switching enhancement. This is in line with what we observed for the kinetics and recovery percentage with films containing conjugates M1-barb, T1-barb, C4-barb, and M2-barb that followed this trend (Tables S8,S9 and Figures S74–S76, Supporting Information). Importantly, this means that a compromise between the polymer chain length and its miscibility with the matrix polymer must be found in order to maximize both the photoswitching enhancement and the transparency of the samples.

Conjugate T1-barb and Barb-1 were also measured in films made from PEMA and PBMA (Figure 4C; Figures S77–S79, Supporting Information). Due to the lower T_g of PEMA and PBMA when compared to PMMA, the inherent switching capacity of Barb-1 at room temperature is already improved so that effects caused by the attached PDMS chain on the photoswitching kinetics are expected to be less pronounced. It was found that this holds true for the relative increase in forward switching rate (time to reach half of the initial absorption value, $t_{A1/2}{}^{P}$, Figure 4C) and the thermal recovery percentage of conjugate T1-barb when compared to Barb-1 in these matrices. This supports the assumption that differences in rigidity between the surrounding polymer and the PDMS local environment are largely responsible for the enhanced photoswitching capability of the conjugates. On the other hand, the analogous pyrazolone-based conjugate T1-pyra also showed enhancement in the forward switching relative to Pyra in PMMA (significantly faster and slightly less open form at PTSS, Figure S80, Supporting Information), while the thermal recovery, however, was not improved but instead slightly decreased. This result highlights again the importance of polymer matrix effects other than rigidity that could become predominant for certain DASAs. Possible complexities for the thermal recovery could arise, for example, from the closed isomer interconverting between different tautomeric forms (enol, zwitterionic, keto)[9,16,17,19,51] for different DASAs with varying stabilization thereof in the macromolecular environment. By analogy, it is well known for spiropyran/spirooxazine photochromes that the merocyanine isomer having different ionic natures (keto vs zwitterionic) and geometric conformations can strongly affect the thermal recovery in polymers and surroundings of different polarities[6,72] demonstrating the need for more systematic in-depth investigations on this aspect for DASA photoswitches.

2.5. DASA-Functionalized PDMS Networks

The hydrosilylation precursor functionalization approach described herein can also be employed to synthesize DASA-functionalized PDMS networks presenting an alternative strategy to improve DASA photoswitching in bulk polymers due to the inherent softness of these materials at room temperature. For this, alkene-and hydrido-functional PDMS precursors were mixed with the alkene-functional aromatic amine 1 and thermally cured at 60°C for three hours inside a Teflon mold using Karstedt's catalyst (**Figure 5**A). The cured network was then immersed into a CH_2Cl_2/HFIP solution (5 vol%) containing the furan adducts for 5 hours resulting in the formation of DASAs that are covalently attached to the PDMS elastomer. The resulting deeply colored networks were washed for several hours in fresh solvents and dried under vacuum. When irradiated with visible light, the DASAs in the dried networks show remarkable
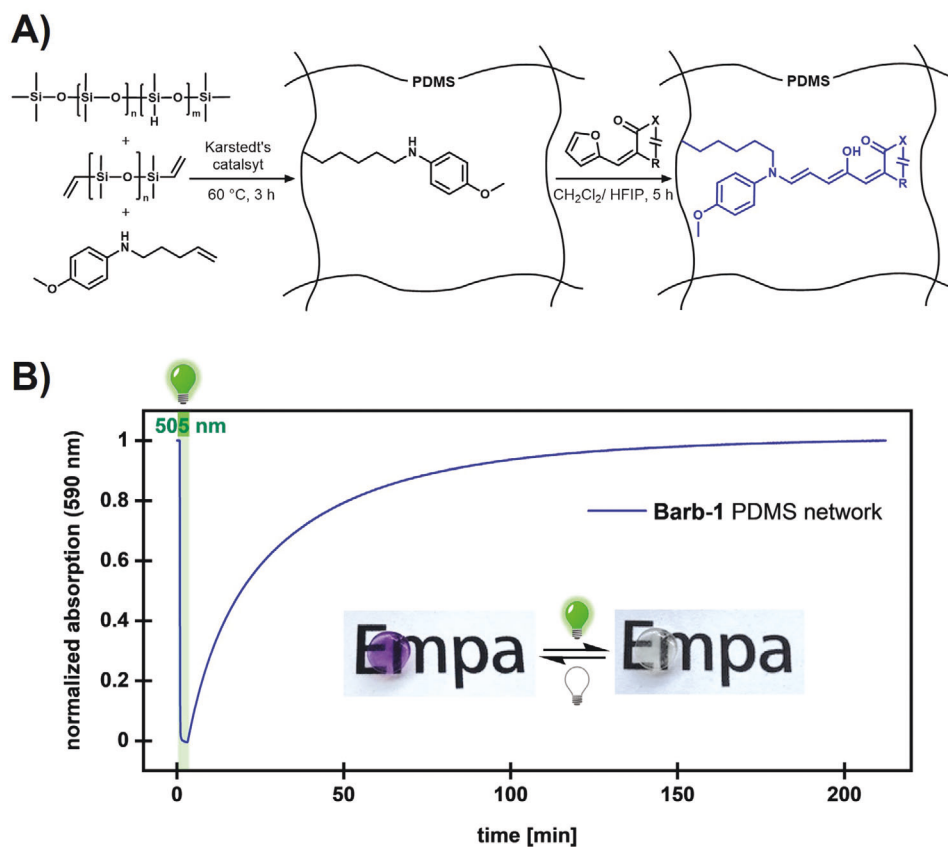
**ADVANCED
SCIENCE NEWS**

www.advancedsciencenews.com

⌈M⌉ **acro-
molecular**
Rapid Communications

www.mrc-journal.de

Figure 5. DASA-functionalized PDMS networks. A) Synthetic route in which alkene-functional DASA-precursor are integrated into the polymer network during network formation via transition metal catalyzed hydrosilylation chemistry followed by DASA formation to yield a DASA-functionalized PDMS network. B) Time-dependent UV–vis spectroscopy (590 nm) on the dry barbituric acid based DASA-PDMS network during illumination (505 nm) and thermal recovery in the dark. Inset shows photographic images of the network before and after photoswitching.

solution-like forward photoswitching speeds with full recovery in the dark (Figure 5B). The thermal recovery is slower ($t_{1/2} = 16$ min) than for Barb-1 in THF solution ($t_{1/2} = 8.4$ min), however, faster than its recovery in more apolar toluene solution ($t_{1/2} \approx 295$ min, Figure S81, Supporting Information). This behavior likely reflects the decreasing medium polarity in this order, since the apparent half-life time of the closed isomer generally decreases with increasing medium polarity in aprotic media.[17,18,51]

The successful network formation and DASA incorporation demonstrate the viability of this approach for creating DASA-functionalized, cross-linked PDMS elastomers. Covalent conjugation of the DASAs to the network prevents aggregation and intermolecular stacking that can impede efficient photoswitching. The soft nature and transparency of PDMS networks allow for fast and efficient DASA photoswitching in the bulk rendering these materials promising candidates for optical applications as DASA-based color changing materials or filters for modulation of other optical properties, such as emission, reflection, or refraction characteristics.

3. Conclusion

Hydrosilylation chemistry was used conjugate DASA-precursors to commercially available linear poly(dimethyl-

methylhydro)siloxanes or to cross-linked PDMS elastomers in order to synthesize a library of DASA-functionalized polymers with varying macromolecular architecture, chain length and linker type. The photoswitching performance of the DASA-PDMS conjugates was studied in solution, blended into polymethacrylate films, and as PDMS networks. Covalent conjugation of low-T_g PDMS to DASA photoswitches was demonstrated to be a simple, yet versatile and effective method to tune and enhance the photoswitching response of DASAs in rigid bulk polymers for reversible modulation of their optical properties. Most DASA-PDMS conjugates dispersed in polymethacrylate films photoisomerized faster and thermally recovered better as compared to the small molecule model DASAs, probably by providing a low-T_g microenvironment around the photoswitches. This is a concept that can be easily expanded to other polymers than PDMS in the future. When selecting a polymer for this approach, phase separation and compatibility issues with the polymer matrix must also be considered, which limits the effective degree of polymerization of the attached polymer that can be utilized for a certain polymer matrix to ensure sufficient homogeneity and transparency. DASA-functionalized PDMS networks, on the other hand, with their intrinsic soft nature, hydrophobicity and transparency, provide an alternative solution for achieving fast and efficient DASA photoswitch-

ing in a bulk material. Furthermore, our results underline the complexity of DASA photoswitching in macromolecular systems, which demonstrates the need for further in-depth investigations on DASA-functionalized polymers in the solid state. Nevertheless, the concept demonstrated herein to localize DASAs in specialized nanoenvironments will likely become key for overcoming current limitations of DASA photoswitches in both bulk materials and aqueous solutions.

4. Experimental Section

Materials and Methods: Poly(dimethyl-methylhydro)siloxanes were obtained from ABCR, Gelest, or Sigma-Aldrich (Table S1, Supporting Information). Other chemicals and solvents were purchased from Sigma-Aldrich, TCI Europe, Polysciences, or Fisher Scientific and were used without further purification unless stated otherwise. Silica gel chromatography was performed using silica gel from Sigma-Aldrich (technical grade, 60 Å pore size, 40–63 μm particle size). Preparative size exclusion chromatography (SEC) was performed on Bio-Beads S-X1 Support (600–14 000 g mol^{-1}, Bio-Rad Laboratories) using distilled THF as mobile phase. ^{1}H and ^{13}C NMR spectra were measured in CDCl$_3$ on a Bruker Avance III 400 (400 MHz) NMR spectrometer at 298 K. Chemical shifts (δ) are reported in ppm and referenced internally from the proteo solvent resonance. Coupling constants (J) are reported in Hz. Abbreviations for the peak multiplicities are s (singlet), d (doublet), dd (doublet of doublet), t (triplet), q (quadruplet), and m (multiplet). For diffusion-edited ^{1}H NMR spectra, 40% gradient strengths were applied to selectively suppress the signals of low molecular weight species. Attenuated total reflection Fourier-transform infrared (ATR FT-IR) spectra were recorded on a Varian 640-IR FT-IR spectrometer equipped with an ATR accessory using neat samples. Absorbance bands are reported as wavenumbers in cm^{-1}. Abbreviations for the relative band intensities are s (strong), m (medium), w (weak). Gel permeation chromatography (GPC) was measured on an Agilent 1100 Series HPLC system on serial coupled PSS SDV 5m 100 Å and PSS SDV 5m 1000 Å columns with THF as the mobile phase (flow rate: 1 mL min^{-1}; temperature: 30 °C). Signals were recorded on a diode array detector (235 nm/360 nm) and a refractive index (RI) detector (at 35 °C) and calibrated with narrow molecular weight PDMS standards. Differential scanning calorimetry (DSC) measurements were done on a NETZSCH DSC 214 Polyma under nitrogen atmosphere at a heating rate of 10 K min^{-1}. The data was analyzed using NETZSCH Proteus-Thermal Analysis software (Version 7.1.0). T_g was determined as the mid-point of the observed transition. Raman imaging was performed with a WITec Alpha300R Raman confocal microscope (WITec, Ulm, Germany) and a Zeiss 100× objective with numerical aperture of 0.90, fiber-coupled to a 785 nm diode laser with maximum power of 125 mW. The Raman scattering was detected with an Ultra-High-Throughput Spectrometer UHTS400 for near infrared (WITec, Ulm, Germany) with a back-illuminated deep depletion 1024×127 CCD Chip with pixel size of 26×26 μm, Peltier cooled to approximately −65 °C and diffraction grating with density of 300 g mm^{-1}. The Raman area mapping was carried out with a resolution of 0.25 μm^2 per pixel, using a measurement time of 2 s per pixel at 40 mW laser power. WITec True Component analysis tool was then used to identify components and create a visual representation of their spatial distribution.

Synthesis of DASAs and Linkers: Synthetic procedures and characterization data of compounds 1 to 5, Barb-1, Barb-2, and Pyra and precursors can be found in Sections S2.1–S2.3 and S4, Supporting Information.

Synthesis of DASA-Precursor Polymers via Hydrosilylation: In a typical procedure, poly(dimethyl-methylhydro)siloxane (0.5–1.5 g) and an approximate twofold molar excess (relative to hydrido functionalities) of 1, 2, or 3 (0.08–0.2 g, 0.4–1.0 mmol) were dissolved in anhydrous toluene (9 mL) in a Schlenk flask equipped with a magnetic stir bar and a septum under nitrogen atmosphere. Karstedst's catalyst (platinum(0)-1,3-divinyl-1,1,3,3-tetramethyldisiloxane complex solution in xylene, Pt ≈2%, Sigma-Aldrich, 40 μL) was added and the reaction mixture was stirred at 60 °C under ni-

trogen atmosphere overnight. After completion, the reaction mixture was filtered through a silica gel plug using CH$_2$Cl$_2$:MeOH (10:1) as eluent. The solvent was then removed in vacuo and the crude product was purified from small molecule impurities via SEC with distilled THF as an eluent and Sudan black as color indicator for the small molecule fraction. Evaporation of the solvent in vacuo yielded the product as yellow/brown viscous oil. Detailed compositions and analytical data are in Sections S2.4 and S4, Supporting Information. Representative characterization data of C4 as follows: ^{1}H NMR (400 MHz, CDCl$_3$, δ/ppm): 6.77 (d, J = 8.8 Hz, 2H; 2× Ar H,), 6.56 (d, J = 8.8 Hz, 2H; 2× Ar H,), 3.74 (s, 3H; O-CH$_3$), 3.05 (t, J = 7.1 Hz, 2H; N-CH$_2$), 1.61-1.58 (m, 2H; CH$_2$), 1.45-1.37 (m, 4H; 2× CH$_2$), 0.52 (t-like m, 2H; Si–CH$_2$), 0.09-0.05 (m, 167 H; Si–CH$_3$); IR (ATR, cm^{-1}): ν = 2960 (w), 1514 (w; ν(Ar C–C)), 1412 (w), 1257 (m; δ(Si–CH$_3$), 1073 (m), 1008 (s; ν(Si–O–Si)), 862 (w), 842 (w), 786 (s; ω(Si–CH$_3$)), 686 (w), 699 (w), 662 (w; ν(Si–O–Si)); GPC: M_n = 3200 g mol^{-1}, Đ = 1.5.

DASA Functionalization: The DASA functionalization was typically done by dissolving the amine-functionalized precursor polymers (0.15 g) in CH$_2$Cl$_2$ (2.4 mL) in a 20 mL glass vial equipped with a stir bar. An excess of furan adducts 4 or 5 (≈0.15 g) was added. HFIP (0.6 mL, i.e., 20 vol%) was added to this mixture for accelerating the reaction and the vial was covered with a plastic lid. After 3 h of stirring at room temperature, the reaction mixture was evaporated to dryness under reduced pressure and the crude product purified from small molecule impurities by SEC with distilled THF as an eluent. Removal of the solvent in vacuo yielded the DASA-PDMS conjugates as dark purple/ blue colored waxy solids or viscous oils. Detailed compositions and analytical data are in the Supporting Information (Sections S2.4 and S4, Supporting Information). C3-barb was synthesized similarly as described before using an excess of 4-methoxy-N-methylaniline. The DASAs exist as a mixture of open and closed isomers at thermal equilibrium. Representative characterization data of C4-barb as follows: ^{1}H NMR (400 MHz, CDCl$_3$, δ/ppm, the signals for the open DASA isomer are reported): 12.5 (s, 1H; OH), 7.32-7.29 (m, 2H; 2× triene CH), 7.12 (d, J = 8.8 Hz, 2H; 2× Ar H), 6.94 (d-like m, "J" = 7.9, 2H; 2× Ar H), 6.66 (d, J = 12.1, 1H; 1× triene CH), 6.21 (broad s, 1H; 1× triene CH), 3.92 (t-like m, "J" = 7.4 Hz; 2× N–CH$_2$ and O–CH$_3$), 3.83-3.80 (m, N–CH$_2$ and O–CH$_3$), 1.61-156 (m; 3× CH$_2$), 1.43-1.26 (m; 4× CH$_2$), 0.93 (t, J = 7.4 Hz; 2× CH$_3$), 0.47 (t-like m; Si–CH$_2$), 0.09-0.05 (m; Si–CH$_3$); IR (ATR, cm^{-1}): ν = 2960 (w), 1683 (w), 1638 (w), 1613 (w), 1541 (w), 1507 (w), 1473 (w), 1410 (w), 1338 (w), 1257 (m), 1200 (w), 1134 (w), 1080 (m), 1008 (s), 862 (w), 841 (w), 788 (s), 727 (m), 693 (m); UV–vis (THF): λ_{max} = 582 nm.

Preparation of DASA-Functionalized Networks: Poly(dimethylsiloxane-co-methylhydrosiloxane) (M_n ≈ 13 000 g mol^{-1}, 3–4 mol% methylhydrosiloxane, Sigma-Aldrich) and alkene-terminated poly(dimethylsiloxane) (M_w ≈ 25 000 g mol^{-1}, iodine value 2.2-3.5, Sigma-Aldrich) were employed for the network synthesis. First, stock solutions of Karstedt's catalyst (platinum(0)-1,3-divinyl-1,1,3,3-tetramethyldisiloxane complex solution in xylene, Pt ≈ 2%, Sigma-Aldrich, 5 μL diluted in 1 mL of anhydrous toluene) and compound 1 (20 mg in 1 mL of anhydrous toluene, 0.10 mol L^{-1}) were prepared. For the curing mixture, alkene-terminated PDMS (1.0 g) was mixed with hydrido-functional PDMS (0.25 g), Karstedt's catalyst stock solution (150 μL), and the precursor stock solution (20 μL, ≈2 μmol of 1). The mixture was filled into 600 μm deep Teflon molds, covered with a glass slide and cured at 60 °C for 1 h. After this, the networks were immersed into CH$_2$Cl$_2$ (150 mL) for 1 h to remove excess reagents and then into a solution of furan adduct 4 or 5 in CH$_2$Cl$_2$ (≈100 mg mL^{-1}) containing 5 vol% HFIP for the DASA functionalization. After 5 h, the purple/blue colored networks were washed by repeated immersion into fresh CH$_2$Cl$_2$ (3×150 mL) for a total of approximately 12 h, dried under vacuum at room temperature overnight and stored in the dark prior to measurements. The washing steps were performed at room temperature with no stirring required. The theoretical DASA functionalization degree assuming 100% conversion in both steps is 1.6 μmol g^{-1}. Representative characterization data for network synthesized with 4: IR (ATR, cm^{-1}): ν = 2961 (w), 2905 (w), 1443 (w), 1412 (w), 1256 (m), 1076 (m), 1007 (s), 863 (w), 784 (s), 696 (w), 660 (w) (Figure S56, Supporting Information); UV–vis: λ_{max} = 577 nm.

Polymethacrylate Film Preparation: PMMA (100 000 g mol^{-1}, atactic beads, Polysciences, Inc.) was used without further purification.

PEMA (515 000 g mol^{-1}, Sigma-Aldrich) and PBMA (inherent viscosity 0.47–0.56 dL g^{-1}, Sigma-Aldrich) were purified by precipitation of a concentrated THF solution of the polymer into ice-cooled MeOH (three times) and subsequent drying of the collected precipitate in vacuo. Thin films were fabricated by a Bungard RDC 15 dip coater on cleaned microscope glass slides (Thermo Fisher Scientific, Menzel-Gläser, 1 mm thickness). The glass slides were cleaned by successive ultrasonication in isopropanol and acetone and then dried in vacuo. The polymethacrylates and DASAs/DASA-PDMS conjugates were dissolved in toluene or toluene/CH$_2$Cl$_2$ mixtures in the dark and dip coated with withdrawal speeds of 70 mm min^{-1} for PBMA, 90 mm min^{-1} for PEMA and 110 mm min^{-1} for PMMA to ensure comparable thickness for all films. Details on compositions and concentrations can be found in Table S6, Supporting Information. The freshly coated films were dried under ambient conditions for 2 min, then removed from the dip coater and subsequently dried at room temperature in vacuum inside a desiccator overnight. The films were stored in the dark prior to measurements. The thickness of the films was measured on a Veeco Dektak 150 profilometer.

Photoswitching Measurements: UV–vis absorbance spectra were recorded on an Agilent Cary 4000 UV–vis spectrophotometer in quartz cuvettes or on an Agilent transmission solid sample holder. For the photoswitching kinetic experiments, multimode optical fiber coupled LEDs were used to irradiate the samples inside the spectrophotometer (M505F3: 505 nm nominal wavelength, 400 μm core fiber output of 11.7 mW; M530F2: 530 nm nominal wavelength, 400 μm core fiber output of 9.6 mW; Thorlabs; Table S2 and Figures S62,S63, Supporting Information). The LEDs were driven by a T-Cube LED Driver (Thorlabs) with the maximum current of 1.2 A. To protect the detector from the intense LED light, dichroic filters were placed in front of it (FD1R for MM505F3 and FD1M for M530F2, 25.4 mm, 2 mm thickness, Thorlabs). The LED light (pump beam) overlaps with the absorbance bands of the respective DASA derivatives, while the probe light from the spectrophotometer (tungsten halogen visible lamp) was set in the transmission range of the filters near λ_{max} (barbituric acid DASA λ_{max} = 583 nm in THF, measured at 590 nm; pyrazolone DASA λ_{max} = 609 nm in THF, measured at 630 nm). The data was normalized to the maximum absorption value at the indicated wavelength. Forward switching was measured under LED illumination perpendicularly from the side of the cuvette or from below the solid samples (dip-coated films and networks) at an angle of incidence of approximately 60° with reference to the normal to the surface and at a distance of ≈0.5 cm (scheme of set-up in Figure S61, Supporting Information). Appropriate holders for the optical fiber head and samples were 3D-printed on an Original Prusa SL1 3D printer in order to keep the distance and angle to the light source constant. The LEDs were turned off manually for monitoring the thermal recovery (note: the probe beam during the thermal recovery was continuously on). Samples were left to equilibrate in the dark for several hours prior to measurements.

Supporting Information

Supporting Information is available from the Wiley Online Library or from the author.

Acknowledgements

Conflict of Interest

The authors declare no conflict of interest.

Data Availability Statement

The data that support the findings of this study are available in the supplementary material of this article.

Keywords

[1] H. Tian, J. Zhang, *Photochromic Materials: Preparation, Properties and Applications*, 1 edition, Wiley-VCH, Weinheim **2016**.
[2] Z. L. Pianowski, *Chem. - Eur. J.* **2019**, *25*, 5128.
[3] J. Boelke, S. Hecht, *Adv. Opt. Mater.* **2019**, *7*, 1900404.
[4] A. Goulet-Hanssens, F. Eisenreich, S. Hecht, *Adv. Mater.* **2020**, *32*, 1905966.
[5] V. A. Krongauz, in *Photochromism* (eds.: H. Duerr, H. Bouas-Laurent), Elsevier Sci, Amsterdam **2003**, p. 793.
[6] G. Such, R. A. Evans, L. H. Yee, T. P. Davis, *J. Macromol. Sci. Polym. Rev.* **2003**, *43*, 547.
[7] F. Ercole, T. P. Davis, R. A. Evans, *Polym. Chem.* **2010**, *1*, 37.
[8] S. Helmy, S. Oh, F. A. Leibfarth, C. J. Hawker, J. Read De Alaniz, *J. Org. Chem.* **2014**, *79*, 11316.
[9] S. Helmy, F. A. Leibfarth, S. Oh, J. E. Poelma, C. J. Hawker, J. Read De Alaniz, *J. Am. Chem. Soc.* **2014**, *136*, 8169.
[10] M. M. Lerch, W. Szymański, B. L. Feringa, *Chem. Soc. Rev.* **2018**, *47*, 1910.
[11] M. M. Lerch, S. J. Wezenberg, W. Szymanski, B. L. Feringa, *J. Am. Chem. Soc.* **2016**, *138*, 6344.
[12] M. Di Donato, M. M. Lerch, A. Lapini, A. D. Laurent, A. Iagatti, L. Bussotti, S. P. Ihrig, M. Medved', D. Jacquemin, W. Szymański, W. J. Buma, P. Foggi, B. L. Feringa, *J. Am. Chem. Soc.* **2017**, *139*, 15596.
[13] M. M. Lerch, M. Medved', A. Lapini, A. D. Laurent, A. Iagatti, L. Bussotti, W. Szymański, W. J. Buma, P. Foggi, M. Di Donato, B. L. Feringa, *J. Phys. Chem. A* **2018**, *122*, 955.
[14] H. Zulfikri, M. A. J. Koenis, M. M. Lerch, M. Di Donato, W. Szymański, C. Filippi, B. L. Feringa, W. J. Buma, *J. Am. Chem. Soc.* **2019**, *141*, 7376.
[15] D. M. Sanchez, U. Raucci, T. J. Martínez, *J. Am. Chem. Soc.* **2021**, *143*, 20015.
[16] J. R. Hemmer, S. O. Poelma, N. Treat, Z. A. Page, N. D. Dolinski, Y. J. Diaz, W. Tomlinson, K. D. Clark, J. P. Hooper, C. Hawker, J. Read De Alaniz, *J. Am. Chem. Soc.* **2016**, *138*, 13960.
[17] N. Mallo, P. T. Brown, H. Iranmanesh, T. S. C. Macdonald, M. J. Teusner, J. B. Harper, G. E. Ball, J. E. Beves, *Chem. Commun.* **2016**, *52*, 13576.
[18] J. R. Hemmer, Z. A. Page, K. D. Clark, F. Stricker, N. D. Dolinski, C. J. Hawker, J. Read De Alaniz, *J. Am. Chem. Soc.* **2018**, *140*, 10425.
[19] N. Mallo, E. D. Foley, H. Iranmanesh, A. D. W. Kennedy, E. T. Luis, J. Ho, J. B. Harper, J. E. Beves, *Chem. Sci.* **2018**, *9*, 8242.
[20] R. Berraud-Pache, E. Santamaría-Aranda, B. De Souza, G. Bistoni, F. Neese, D. Sampedro, R. Izsák, *Chem. Sci.* **2021**, *12*, 2916.
[21] M. Clerc, F. Stricker, S. Ulrich, M. Sroda, N. Bruns, L. F. Boesel, J. Read De Alaniz, *Angew. Chem., Int. Ed.* **2021**, *60*, 10219.
[22] N. R. B. Boase, *Macromol. Rapid Commun.* **2020**, *41*, 2000305.
[23] S. Ulrich, J. R. Hemmer, Z. A. Page, N. D. Dolinski, O. Rifaie-Graham, N. Bruns, C. J. Hawker, L. F. Boesel, J. Read De Alaniz, *ACS Macro Lett.* **2017**, *6*, 738.

[24] S. Ulrich, X. Wang, M. Rottmar, R. M. Rossi, B. J. Nelson, N. Bruns, R. Müller, K. Maniura-Weber, X.- H. Qin, L. F. Boesel, *Small* **2021**, *17*, 2101337.

[25] L. Mao, Z. Wang, Y. Duan, C. Xiong, C. He, X. Deng, Y. Zheng, D. Wang, *ACS Nano* **2021**, *15*, 10384.

[26] S. Singh, K. Friedel, M. Himmerlich, Y. Lei, G. Schlingloff, A. Schober, *ACS Macro Lett.* **2015**, *4*, 1273.

[27] G. Sinawang, B. Wu, J. Wang, S. Li, Y. He, *Macromol. Chem. Phys.* **2016**, *217*, 2409.

[28] F.-Y. Tang, J.-N. Hou, K.-X. Liang, Y. Liu, L. Deng, Y.-N. Liu, *New J. Chem.* **2017**, *41*, 6071.

[29] B. Wu, T. Xue, W. Wang, S. Li, J. Shen, Y. He, *J. Mater. Chem. C* **2018**, *6*, 8538.

[30] H. Zhao, D. Wang, Y. Fan, M. Ren, S. Dong, Y. Zheng, *Langmuir* **2018**, *34*, 15537.

[31] S. H. Mostafavi, W. Li, K. D. Clark, F. Stricker, J. R. D. Alaniz, C. J. Bardeen, *Macromolecules* **2019**, *52*, 6311.

[32] M. Nau, D. Seelinger, M. Biesalski, *Adv. Mater. Interfaces* **2019**, *6*, 1900378.

[33] D. E. Nánási, A. Kunfi, Á. Ábrahám, P. J. Mayer, J. Mihály, G. F. Samu, É. Kiss, M. Mohai, G. London, *Langmuir* **2021**, *37*, 3057.

[34] S. Seshadri, S. J. Bailey, L. Zhao, J. Fisher, M. Sroda, M. Chiu, F. Stricker, M. T. Valentine, J. Read De Alaniz, M. E. Helgeson, *Langmuir* **2021**, *37*, 9939.

[35] S. O. Poelma, S. S. Oh, S. Helmy, A. S. Knight, G. L. Burnett, H. T. Soh, C. J. Hawker, J. Read De Alaniz, *Chem. Commun.* **2016**, *52*, 10525.

[36] T. Senthilkumar, L. Zhou, Q.i Gu, L. Liu, F. Lv, S. Wang, *Angew. Chem., Int. Ed.* **2018**, *57*, 13114.

[37] O. Rifaie-Graham, S. Ulrich, N. F. B. Galensowske, S. Balog, M. Chami, D. Rentsch, J. R. Hemmer, J. Read De Alaniz, L. F. Boesel, N. Bruns, *J. Am. Chem. Soc.* **2018**, *140*, 8027.

[38] J. E. Yap, L. Zhang, J. T. Lovegrove, J. E. Beves, M. H. Stenzel, *Macromol. Rapid Commun.* **2020**, *41*, 2000236.

[39] Y. Zhang, X. Zhang, W. Chen, Y. He, Y. Liu, H. Ju, *J. Controlled Release* **2021**, *336*, 469.

[40] J. Lin, H. Ma, Z. Wang, S. Zhou, B. Yan, F. Shi, Q. Yan, J. Wang, H. Fan, J. Xiang, *Macromol. Rapid Commun.* **2021**, *42*, 2100318.

[41] A. Balamurugan, H.-I. Lee, *Macromolecules* **2016**, *49*, 2568.

[42] B. P. Mason, M. Whittaker, J. Hemmer, S. Arora, A. Harper, S. Alnemrat, A. Mceachen, S. Helmy, J. Read De Alaniz, J. P. Hooper, *Appl. Phys. Lett.* **2016**, *108*, 041906.

[43] D. Zhong, Z. Cao, B.o Wu, Q. Zhang, G. Wang, *Sens. Actuators, B* **2018**, *254*, 385.

[44] Q. Chen, Y. J. Diaz, M. C. Hawker, M. R. Martinez, Z. A. Page, S. Xiao-An Zhang, C. J. Hawker, J. Read De Alaniz, *Macromolecules* **2019**, *52*, 4370.

[45] S. Ulrich, S. O. Moura, Y. Diaz, M. Clerc, A. G. Guex, J. R. De Alaniz, A. Martins, N. M. Neves, M. Rottmar, R. M. Rossi, G. Fortunato, L. F. Boesel, *Sens. Actuators, B* **2020**, *322*, 128570.

[46] J. Lee, M. M. Sroda, Y. Kwon, S. El-Arid, S. Seshadri, L. F. Gockowski, E. W. Hawkes, M. T. Valentine, J. Read De Alaniz, *ACS Appl. Mater. Interfaces* **2020**, *12*, 54075.

[47] J. E. Yap, N. Mallo, D. S. Thomas, J. E. Beves, M. H. Stenzel, *Polym. Chem.* **2019**, *10*, 6515.

[48] S. Singh, P. Mai, J. Borowiec, Y. Zhang, Y. Lei, A. Schober, *R. Soc. Open Sci.* **2018**, *5*, 180207.

[49] B. F. Lui, N. T. Tierce, F. Tong, M. M. Sroda, H. Lu, J. Read De Alaniz, C. J. Bardeen, *Photochem. Photobiol. Sci.* **2019**, *18*, 1587.

[50] M. M. Lerch, M. Di Donato, A. D. Laurent, M. Medved', A. Iagatti, L. Bussotti, A. Lapini, W. J. Buma, P. Foggi, W. Szymański, B. L. Feringa, *Angew. Chem., Int. Ed.* **2018**, *57*, 8063.

[51] M. M. Sroda, F. Stricker, J. A. Peterson, A. Bernal, J. Read De Alaniz, *Chem. - Eur. J.* **2021**, *27*, 4183.

[52] J. Volarić, W. Szymanski, N. A. Simeth, B. L. Feringa, *Chem. Soc. Rev.* **2021**, *50*, 12377.

[53] N. Mallo, A. Tron, J. Andréasson, J. B. Harper, L. S. D. Jacob, N. D. Mcclenaghan, G. Jonusauskas, J. E. Beves, *ChemPhotoChem* **2020**, *4*, 407.

[54] R. Saha, A. Devaraj, S. Bhattacharyya, S. Das, E. Zangrando, P. S. Mukherjee, *J. Am. Chem. Soc.* **2019**, *141*, 8638.

[55] L. Payne, J. D. Josephson, R. S. Murphy, B. D. Wagner, *Molecules* **2020**, *25*, 4928.

[56] S. Mukhopadhyay, A. Sarkar, S. Ghoshal, P. Sarkar, K. Dhara, P. Chattopadhyay, *J. Phys. Chem. B* **2021**, *125*, 7222.

[57] F. Sun, X. Xiong, A. Gao, Y. Duan, L. Mao, L. Gu, Z. Wang, C. He, X. Deng, Y. Zheng, D. Wang, *Chem. Eng. J.* **2022**, *427*, 132037.

[58] R. A. Evans, G. K. Such, *Aust. J. Chem.* **2005**, *58*, 825.

[59] R. A. Evans, T. L. Hanley, M. A. Skidmore, T. P. Davis, G. K. Such, L. H. Yee, G. E. Ball, D. A. Lewis, *Nat. Mater.* **2005**, *4*, 249.

[60] G. K. Such, R. A. Evans, T. P. Davis, *Macromolecules* **2006**, *39*, 1391.

[61] N. Malic, J. A. Campbell, A. S. Ali, M. York, A. D'souza, R. A. Evans, *Macromolecules* **2010**, *43*, 8488.

[62] N. Malic, J. A. Campbell, R. A. Evans, *Macromolecules* **2008**, *41*, 1206.

[63] F. Ercole, N. Malic, T. P. Davis, R. A. Evans, *J. Mater. Chem.* **2009**, *19*, 5612.

[64] F. Ercole, T. P. Davis, R. A. Evans, *Macromolecules* **2009**, *42*, 1500.

[65] F. Ercole, N. Malic, S. Harrisson, T. P. Davis, R. A. Evans, *Macromolecules* **2010**, *43*, 249.

[66] J. E. Mark, *Polymer Data Handbook*, Oxford University Press, New York **1999**.

[67] D. Troegel, J. Stohrer, *Coord. Chem. Rev.* **2011**, *255*, 1440.

[68] A. Chechelska-Noworyta, M. Owińska, M. Hasik, *J. Organomet. Chem.* **2019**, *898*, 120866.

[69] K. Stranius, K. Börjesson, *Sci. Rep.* **2017**, *7*, 41145.

[70] L. Jayes, A. P. Hard, C. Séné, S. F. Parker, U. A. Jayasooriya, *Anal. Chem.* **2003**, *75*, 742.

[71] A. D. Laurent, M. Medveď, D. Jacquemin, *ChemPhysChem* **2016**, *17*, 1846.

[72] L. Kortekaas, W. R. Browne, *Chem. Soc. Rev.* **2019**, *48*, 3406.